Dynamics of kicked particles in a double-barrier structure

Harinder Pal[1,*] and M. S. Santhanam[2,†]
[1]*Physical Research Laboratory, Navrangpura, Ahmedabad 380 009, India*
[2]*Indian Institute of Science Education and Research, Pashan Road, Pune 411 021, India*
(Received 10 August 2010; published 24 November 2010)

We study the classical and quantum dynamics of periodically kicked particles placed initially within an open double-barrier structure. This system does not obey the Kolmogorov-Arnold-Moser (KAM) theorem and displays chaotic dynamics. The phase-space features induced by non-KAM nature of the system lead to dynamical features such as the nonequilibrium steady state, classically induced saturation of energy growth and momentum filtering. We also comment on the experimental feasibility of this system as well as its relevance in the context of current interest in classically induced localization and chaotic ratchets.

DOI: 10.1103/PhysRevE.82.056212 PACS number(s): 05.45.Mt, 68.65.Fg, 05.45.Pq

I. INTRODUCTION

Periodically kicked rotor is a popular model that has served as a paradigm to understand Hamiltonian chaos both in the classical and quantum regimes [1]. This was originally introduced as a simple model for dynamical chaos but was sufficiently general to cover many physical situations. For instance, problems such as the hydrogen atom in microwave fields and motion of a comet around the sun driven by a suitable planet can be reduced to that of kicked rotor [2]. This system is also paradigmatic for another important reason; it obeys the Kolmogorov-Arnold-Moser (KAM) theorem [3]. This implies that as a control parameter is varied, the transition from regularity to chaos occurs progressively by the breaking down of invariant curves in phase space. Once all the invariant curves are broken down, diffusive global transport of particles in phase space becomes possible. In the corresponding quantum regime, this classical diffusive transport is inhibited by the onset of dynamical localization [4]. This was experimentally realized in the laboratory with cold atoms in optical lattices [5] and was the basis for theoretical and experimental realization of chaotic ratchets in recent times [6].

On the other hand, there are other physical systems that exhibit classical chaos but violate the KAM theorem, the so-called non-KAM systems. This class includes the kicked harmonic oscillator [7] and the kicked particle in infinite square-well potential [8,10]. In both these cases, when a parameter is varied, the invariant curves are replaced by stochastic webs [7], an intricate chain of islands and globally connected channels through which particle transport becomes possible. Non-KAM type is also relevant for an important class of physical systems, namely, the dynamics of particles in quantum wells and barrier structures. To date, non-KAM systems have been experimentally realized in semiconductor superlattices in tilted magnetic fields in which the enhanced conductivity could be attributed to non-KAM chaos [11]. Further, measurement of the Lochschmidt echo using a non-KAM system, namely, the ion trap with harmonic potential in the presence of a kicking field [12], has also been proposed. In spite of this, very few non-KAM systems have been investigated and they have not been explored in sufficient details.

Another motivation for this work stems from the considerable interest in recent times in the dynamics of condensates placed in finite box-type potentials acted upon by a periodically kicking field. In a recent experiment, Henderson *et al.* [13] constructed a quasi-one-dimensional finite box using a combination of optical and magnetic trap, with the Bose-Einstein condensates (BECs) in the box receiving periodic kicks. This setup was used to study the effect of atomic interactions on the transport of BECs. In place of the dynamical localization they observed a classical saturation in the energy of BECs due to a balance between the energy gained from kicks and the energy lost by leakage of BECs over the finite barrier [13]. Apart from this, a series of experiments [14] that studied the transport of BECs in the presence of disordered potential has reported such classically induced energy saturation effects. Then the questions are whether or not it is possible to observe such classically induced energy saturation in chaotic systems without interparticle interactions and what its mechanism would be. We show that a kicked particle in finite well type potential that we study in this paper shows this feature and we discuss its mechanism. It is also relevant to point out that following the achievement of BECs in the optical box trap [15], theoretical investigations of resonance and antiresonance behaviors and its relation to the KAM and non-KAM type dynamics for BECs in one-dimensional (1D) infinite well have also been performed [16]. Further, experiments exploring the interface of nonlinear dynamics of electrons in 1D quantum well irradiated at terahertz frequencies have already been reported [17].

Although non-KAM type dynamics is a generic feature in physical systems, such as the potential wells, not much work has been done on this class of problems. However, on the theoretical front, infinite square-well potential confining a delta-kicked particle has been studied [8,10]. In light of recent attempts to study chaotic ratchets [6], in both the classical and quantum sense, it would be useful to open the potential to allow for particle transport. This could lead to chaotic ratchets that can utilize non-KAM features of its classical system for directed transport. In this paper, we study a periodically kicked particle initially held in between

*harinder@prl.res.in
†santh@iiserpune.ac.in

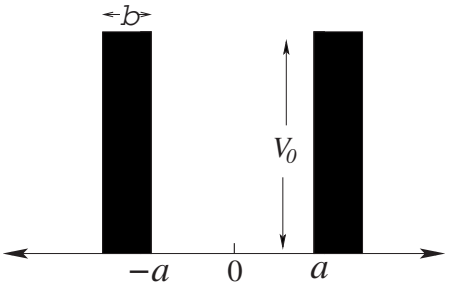

FIG. 1. Schematic of the stationary part of the potential. The width of each barrier is b. The well region has the width $2a$.

a finite double-barrier structure. Double barrier heterostructures play an important role in electronic devices that use resonant tunneling diodes [18], though without the kicking potential. Primarily we present numerical explorations of this problem to study its rich dynamical features. In Sec. II, we introduce our model and in subsequent sections we discuss the classical and quantum dynamics of this system.

II. KICKED PARTICLE IN DOUBLE BARRIER

We consider the dynamics of a noninteracting particle initially located in between two potential barriers each of height V_0 and width b distant $2a$ apart (see Fig. 1). The particle is further subjected to flashing δ kicks of period T generated by a spatially periodic potential field of wavelength λ. Amplitude ϵ of the kicking field is generally referred to as kick strength. The classical Hamiltonian of the system is

$$\tilde{H} = \frac{\tilde{p}^2}{2m} + \tilde{V}_{sq} + \tilde{\epsilon}\cos\left(\frac{2\pi\tilde{x}}{\lambda} + \phi\right)\sum_{n=-\infty}^{\infty}\delta(\tilde{t} - nT), \qquad (1)$$

where $\tilde{V}_{sq} = \tilde{V}_0[\Theta(\tilde{x}+\tilde{b}+a) - \Theta(\tilde{x}+a) + \Theta(\tilde{x}-a) - \Theta(\tilde{x}-a-\tilde{b})]$, $\Theta(\cdot)$ is the unit step function, and ϕ is the phase of the kicking field. The set of canonical transformations given by

$$\tilde{t} = tT, \quad \tilde{x} = \lambda\frac{(x-\phi)}{2\pi}, \quad \tilde{p} = \frac{pTE_c}{\lambda\pi},$$

$$\tilde{H} = \frac{HE_c}{2\pi^2}, \quad \tilde{\epsilon} = \frac{\epsilon E_c T}{2\pi^2}, \quad \tilde{V}_0 = \frac{V_0 E_c}{2\pi^2}, \quad \tilde{b} = \frac{\lambda}{2\pi}b, \qquad (2)$$

with $E_c = m\lambda^2/2T^2$ leads to a new dimensionless Hamiltonian,

$$H = \frac{p^2}{2} + V_{sq} + \epsilon\cos(x)\sum_{n=-\infty}^{\infty}\delta(t-n). \qquad (3)$$

In this, $V_{sq} = V_0[\Theta(x-\phi+b+R\pi) - \Theta(x-\phi+R\pi) + \Theta(x-\phi-R\pi) - \Theta(x-\phi-R\pi-b)]$, with $R = 2a/\lambda$ being the ratio of the distance between the barriers to the wavelength of the kicking field. The classical dynamics of the system depends on five parameters, namely, ϵ, R, b, V_0, and ϕ. Of these, R, b, and ϕ determine the positions of discontinuities in the potential (position of the wall boundaries) at $\mathbf{B} = \{x_l - b, x_l, x_r, x_r + b\}$, where $x_l = -R\pi + \phi$ and $x_r = R\pi + \phi$. Note that if $\phi = 0$, then $x_l = -x_w$ and $x_r = x_w$ with $x_w = R\pi$. Thus, the qualitative nature of the classical dynamics depends on the positions of wall boundaries collectively denoted by $\mathbf{B}$, the kick strength ϵ, and potential height V_0. In this paper (except in Sec. III C), we set $\phi = 0$ which makes the potential symmetric about $x = 0$. It is useful to write Eq. (3) as

$$H = H_0 + V_{sq}(x), \qquad (4)$$

where $H_0 = p^2/2 + \epsilon\cos(x)\Sigma_{n=-\infty}^{\infty}\delta(t-n)$ leads to standard map defined on the infinite plane. Note that if $V_{sq}(x) = V_0$, a constant, then the Hamiltonian equations will not have the potential term and the dynamics would be completely governed by H_0.

III. CLASSICAL DYNAMICS

A. Classical map

The Hamiltonian in Eq. (3) is classically integrable for $\epsilon = 0$. This corresponds to free motion in the presence of two potential barriers and hence it is possible to obtain a transformation to action-angle variables. For $\epsilon > 0$, the system is nonintegrable and can even display abrupt transition to chaotic dynamics with mixed phase space depending on the values of R, b, and ϕ. It is convenient to think of the system as being entirely governed by H_0 and then incorporate effect of discontinuities in V_{sq} through appropriate boundary conditions. This leads to the following map:

$$p_n = p_{n-1} + \epsilon\sin(x_{n-1}), \qquad (5a)$$

$$x_n = x_{n-1} + p_n,$$

$$\begin{pmatrix} p_n \\ x_n \end{pmatrix} \to \hat{\mathcal{R}}\begin{pmatrix} p_n \\ x_n \end{pmatrix}. \qquad (5b)$$

Equation (5a) represents the effect of H_0 and is identical to the standard map. In Eq. (5b), the operator $\hat{\mathcal{R}} = \hat{\mathcal{R}}_k \ldots \hat{\mathcal{R}}_2\hat{\mathcal{R}}_1$ represents the effect due to k encounters of the particle, in between two kicks, with the discontinuities of V_{sq} at positions represented by $B_1, B_2, \ldots, B_k$, respectively. Depending on the energy, each of these k encounters could either be a reflection (sign of momentum changes) or refraction (magnitude of momentum changes) at $B_i \in \mathbf{B}$, $i = 1, 2, \ldots, k$.

The map in Eq. (5) would be complete if the operator $\hat{\mathcal{R}}_i$, which incorporates the effect of ith discontinuity encountered, is explicitly written down. Between successive kicks applied at times n and $n+1$, we denote the state of the particle after incorporating effect of ith encounter with a boundary B_i by $\binom{x_n^i}{p_n^i}$. We define $]x_s^i, x_n^i[$ with $i = 0, 1, \ldots, k$ as the path; starting from x_s^i, a particle would traverse between the two kicks after encountering ith discontinuity if there were no discontinuities to be faced until the next kick. For $i = 0$, x_n^i would simply be x_{n-1} and would be equal to B_i for $i > 0$. x_n^0 and p_n^0 to be used in boundary conditions would simply be x_n and p_n obtained directly from Eq. (5a). Boundary conditions defined by Eq. (6) below are applied k times until $]x_s^k, x_n^k[\cap \mathbf{B} = \varnothing$. If E_n denotes the energy of the system at nth

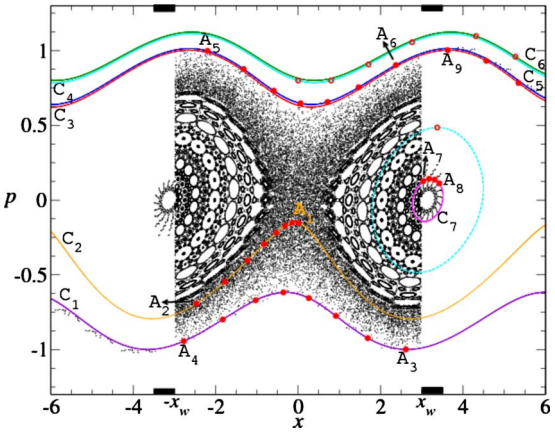

FIG. 2. (Color online) Stroboscopic Poincare section (black) for $R=0.95$, $\epsilon=0.15$, $V_0=0.5$, $\phi=0$, and $b=0.5$. All the continuous curves (in color) marked C_1-C_6 are for the corresponding standard map with kick strength of 0.15. The black box at position $x=\pm x_w$ indicates the width b of the barrier. The solid circles (in red) show a trajectory starting from A_1 until it exits the potential well at A_9. The time-ordered sequence of the trajectory is A_1 to A_2, reflection at $-x_w$, A_3 to A_4, reflection at x_w, A_5 to A_6, cross the boundary at x_w, A_7 to A_8, and cross the boundary at x_w+b, exit the potential at A_9. See text for details.

kick, then for $E_n \leq V_0$ (reflective boundary condition), we obtain

$$\hat{\mathcal{R}}_i \begin{pmatrix} x_n^{i-1} \\ p_n^{i-1} \end{pmatrix} = \begin{pmatrix} 2B_i - x_n^{i-1} \\ -p_n^{i-1} \end{pmatrix}. \tag{6a}$$

For $E_n > V_0$ (refractive boundary condition), we get

$$\hat{\mathcal{R}}_i \begin{pmatrix} x_n^{i-1} \\ p_n^{i-1} \end{pmatrix} = \begin{pmatrix} B_i + \dfrac{(x_n^{i-1} - B_i)p_n^i}{p_n^{i-1}} \\ \dfrac{p_n^{i-1}}{|p_n^{i-1}|}\sqrt{(p_n^{i-1})^2 - \dfrac{2V_0 V_{diff}}{|V_{diff}|}} \end{pmatrix}. \tag{6b}$$

In this, we have used $V_{diff}=V(x_n^{i-1})-V(x_s^{i-1})$. Thus, the dynamics of system in Eq. (3) can be described by the standard map with $-\infty \leq x_n, p_n \leq \infty$ [Eq. (5)] subjected to potential barriers [Eq. (5b)]. Notice that by putting $V_0=0$ in Eq. (6b), we obtain $\hat{\mathcal{R}}_i=\mathbf{I}$ for all i, where $\mathbf{I}$ is the identity matrix of order 2. Then $\hat{\mathcal{R}}=\mathbf{I}$ and, as expected, Eq. (5) reduces to standard map for $V_0=0$. Thus, transformations (5b) and (6) can be viewed as deviation from standard map dynamics induced after each encounter of the particle with the a discontinuity of potential V_{sq}.

B. Phase space features

Figure 2 shows a stroboscopic section obtained by evolving the map in Eq. (5) for uniformly distributed initial conditions in $x \in (-x_w, x_w), p \in (-p_c, p_c)$, where $p_c=\sqrt{2mV_0}$ is the minimum momentum required for barrier crossing. In this paper, we have chosen kick strength $\epsilon \ll 1$ such that the corresponding standard map displays only KAM curves. First, a striking feature is the absence of invariant curves and the appearance of a mixed phase space. This is in stark contrast with the standard map which displays mostly quasiperiodic orbits for kick strengths of this order. This figure also shows snap shots (solid circles in red) of trajectory in-between successive encounters with the discontinuities at B. Clearly, the evolution between two successive encounters with the boundaries is confined to a trajectory that is identical with one of the quasiperiodic orbits of the corresponding standard map [obtained from Eq. (5) with $V_0=0$] shown as continuous lines in the figure. Due to V_{sq}, particle breaks away from one quasiperiodic orbit and joins another at each encounter with the boundaries. This leads to absence of quasiperiodic orbits and development of mixed phase space comprising intricate chains of islands embedded in chaotic sea. We illustrate the effects of discontinuities in Fig. 2 by following a typical initial condition marked A_1 in the chaotic layer. This evolves to A_2 on the invariant curve C_2 of the corresponding standard map. After a long time, this point appears on the curve C_1 and goes from A_3 to A_4. After a reflection at $-x_w$, it goes from A_5 to A_6 on C_3. Then it shifts to the barrier region (x_w, x_w+b) and moves on C_7 from A_7 to A_8. Depending on the winding number of the orbit in (x_w, x_w+b), the particle could have gone back to region between the barriers or escape from the finite well. In the present example, it makes its escape out of two barrier structures and its state meets the curve C_5 at A_9. Once the particle has escaped, its state evolves on same curve as $n \to \infty$. Thus, system displays KAM behavior for $|x| > x_w+b$.

The absence of quasiperiodic orbits can be attributed to the nonanalyticity of V_{sq} which violates the assumptions of KAM theorem. Thus, the non-KAM nature of system leads to onset of chaos even for $\epsilon < 1$. The initial conditions starting from chaotic layer will diffuse in momentum space. Some of these initial conditions which reach the set of quasiperiodic orbits $C(\mu)$ (μ being the winding number) of the corresponding standard map which overlaps the region $|p| > p_c$ can escape from the finite well. As μ increases, this overlap also increases and hence the escape probability is larger. This implies that there must exist μ_c such that the states on any $C(\mu)$, with $\mu > \mu_c$, will definitely cross the barrier and escape from the well. These orbits do not encounter the discontinuities in the potential multiple times and hence the energy of the particles evolving on such quasiperiodic orbits will not diffuse. Figure 2 also shows the trajectory of a particle (open circles in red on the curves C_5 and C_6) in such nondiffusive region. As seen in Fig. 2, the discontinuities at x_w and x_w+b relocate the incoming particle from C_5 (μ_5) to another orbit C_6 (μ_6), where μ_5 and μ_6 are their winding numbers, respectively. As shown in Appendix A, when $b \to 0$, the effect of these discontinuities decreases and deviation between two orbits measured as $(\mu_6-\mu_5) \to 0$. This results in the appearance of regular orbits (see Fig. 3) identical to those of the standard map except that the former have imperceptible discontinuities wherever there is a discontinuity in potential. In other words, refraction becomes identity operation as $b \to 0$. Thus, the system shows regular dynamics outside region enclosed between curves $C_{\pm}(\mu_c)$ (see Fig. 3) as $b \to 0$. Note that the limits on chaotic phase space in terms of μ on positive and negative sides of mo-

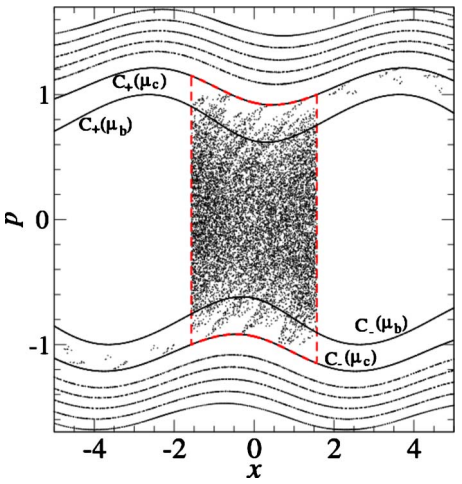

FIG. 3. (Color online) Stroboscopic plot [excluding $C_{\pm}(\mu_b)$] for $b=10^{-3}$ and $R=0.5$. All the other parameters are same as in Fig. 2. Dashed line (in red) represents the boundary of region $\mathcal{M}$. The mild scatter of points just below $C_+(\mu_c)$ and just above $C_-(\mu_c)$ represents the particles escaping out of the well (whose initial states were in $\mathcal{M}$). The curves $C_+(\mu_b)$ and $C_-(\mu_b)$ shown here are used in Sec. V B.

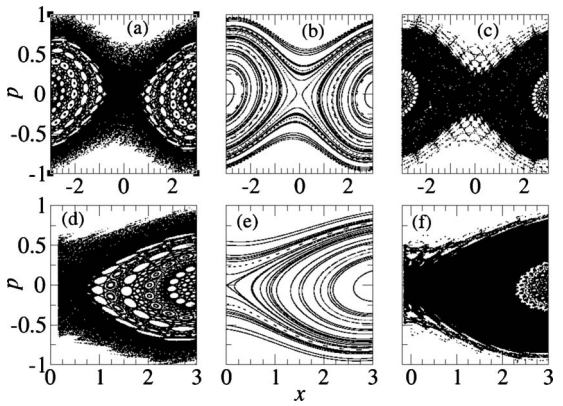

FIG. 4. Stroboscopic Poincare section for the Hamiltonian in Eq. (1) showing the region $x \in (x_l, x_r), p \in (-p_c, p_c)$ for $b=0, \epsilon=0.15, V_0=0.5$. The other parameters are (a) $R=0.95, \phi=0$ (b) $R=1.0, \phi=0$, (c) $R=1.05, \phi=0$, (d) $R=0.45, \phi=\pi/2$, (e) $R=0.5, \phi=\pi/2$, and (f) $R=0.55, \phi=\pi/2$.

mentum are identical due to assumption that $\phi=0$. Limits on the chaotic phase space would exist even otherwise, though these would not be identical on both sides of $p=0$. The discussions in this section can be summarized as follows: we can define a phase-space region $\mathcal{M}[|x|<x_w+b; |p(x)|<p(x;\mu_c)]$ such that system has mixed phase space inside $\mathcal{M}$ in general and regular dynamics outside it. Here, $p(x;\mu_c)$ is momentum of any state on the curve $C_+(\mu_c)$ at position x. In Fig. 3, a close numerical approximation of the region $\mathcal{M}$ is highlighted by the red dashed line.

We remark that for $b \to 0$, the phase-space structures inside $\mathcal{M}$ are identical to those of well map that describes the dynamics of δ-kicked particle in an infinite well [8]. This is to be expected since the well map has only reflective boundaries for $|p| \leq \infty$. Further, the well map is hyperbolic for $R<0.5$ for any $\epsilon>0$. The Hamiltonian in Eq. (1) also displays complete chaos for $R<0.5$ inside $\mathcal{M}$. This is seen in Fig. 3 as no regular structures are visible in this region to the accuracy of our calculations. The region defined by $\mathcal{M}$ is determined by the positions of potential discontinuities **B** and $C_{\pm}(\mu_c)$. It can be shown that $C_{\pm}(\mu_c)$ will remain close to $\pm p_c(=\pm\sqrt{2mV_0})$ when $b \to 0$ for any ϵ for which standard map has mostly regular phase space. Thus, the extent of chaotic region will depend grossly on the positions **B** and height V_0 of the barriers only. This implies that it is possible to engineer chaos in a desired region by varying these parameters.

C. KAM-like behavior: Role of symmetries

In this section, we explore the conditions under which KAM or non-KAM type of dynamics can be realized in the system. In Eq. (1), the nonanalyticity of V_{sq} violates the assumptions of the KAM theorem. Hence, generically we expect this system to display the signatures of non-KAM system such as the stochastic webs instead of quasiperiodic orbits and an abrupt transition to chaos. These features are shown in Figs. 4(a), 4(c), 4(d), and 4(f). However, we show that even in the presence of nonanalyticity in V_{sq}, quasiperiodic orbits similar to that in a KAM system can be realized if certain symmetry conditions are satisfied.

As argued before, until interrupted by the barriers, the dynamics is confined to a particular invariant curve of the corresponding standard map. We recall that corresponding to every trajectory C_+ of standard map with $p_n>0$, there exists one and only one trajectory C_- with $p_n<0$, such that a particle will evolve on these trajectories in exactly the same way but in opposite direction. As shown in Appendix B, consider the (R, ϕ) pairs for which the condition

$$\pm R\pi + \phi = l2\pi, \quad l \in \mathbb{Z}, \tag{7}$$

is satisfied. When Eq. (7) is satisfied, application of $\hat{\mathcal{R}}_i$ takes a particle from C_+ to C_- and application of $\hat{\mathcal{R}}_{i+1}$ brings it back to C_+. This leads to quasiperiodic behavior in which the particle is confined to a pair of tori. This quasiperiodic orbit undergoes smooth deformation just like in a KAM system until it breaks for large kick strengths. Hence, we call this KAM-like behavior for its striking resemblance to the qualitative behavior of a KAM system. In general, there exist infinite (R, ϕ) pairs for which KAM-like dynamical behavior can be recovered in this system. In Figs. 4(b) and 4(d), we show the sections for $R=1, \phi=0$ and $R=0.5, \phi=\pi/2$ for which KAM-like behavior is obtained. In Figs. 4(a), 4(c), 4(d), and 4(f), we also show cases where Eq. (7) is not satisfied and hence for $|p|<p_c$ stochastic webs and chaotic regions are seen.

Symmetry related invariant curves such as C_+ and C_- are due to the symmetry of the kicking field about any $x=m\pi+\phi$, where m is an integer. It turns out that when Eq. (7) is satisfied, kicking field is symmetric about x_w and x_{-w}. The existence of KAM-like behavior in the presence of nonanalytic potential can be attributed to the existence of centers of symmetry of kicking field at $-x_w$ and x_w.

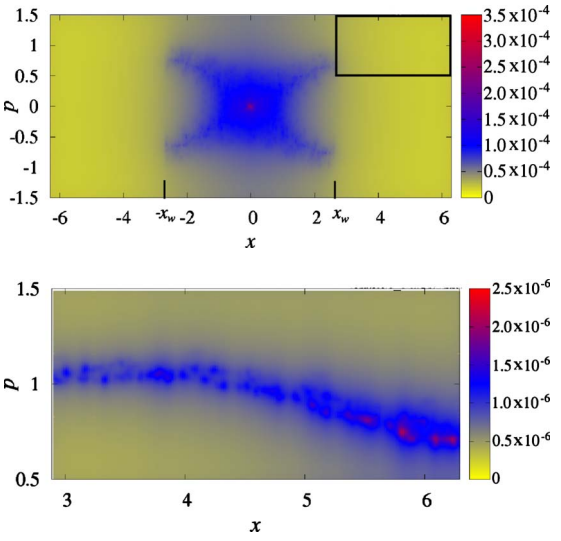

FIG. 5. (Color online) (Top) The Husimi distribution for evolved wave packet. Initial wave function corresponds to $Q(x_0,p_0,n)$ sharply localized inside the chaotic region around (0,0). In the gray scale version, the regions with larger values of the Husimi distribution function are grossly represented by the darker areas. It shows that the function decays very steeply outside $[x_{-w},x_w]$ and acquires negligible values compared to those for region inside $[x_{-w},x_w]$. We have taken $\hbar_s=0.0025$, $R=0.85$, $b=0.2$, $\epsilon=0.15$, $V_0=0.5$, and $\phi=0$. (Bottom) Enlarged and better resolved view of inset from figure on the top shows path followed by probability density outside the barrier region.

IV. QUANTUM DYNAMICS

In this section, we discuss the quantum simulations of the system. We start by writing down the time-dependent Schrödinger equation corresponding to the scaled Hamiltonian in Eq. (3),

$$i\hbar_s\frac{\partial\psi}{\partial t}=\left[\frac{-\hbar_s^2}{2}\frac{\partial^2}{\partial x^2}+V_{sq}+\epsilon\cos x\sum_n \delta(t-n)\right]\psi. \quad (8)$$

Scaled Planck's constant is $\hbar_s=2\pi^2\hbar/E_cT$. This being a kicked system, we can obtain the one-period Floquet operator,

$$\hat{U}=\exp\left(-\frac{i\epsilon}{\hbar_s}\cos\hat{x}\right)\exp\left(-\frac{i}{\hbar_s}\left[\frac{\hat{p}^2}{2}+\hat{V}_{sq}\right]\right), \quad (9)$$

such that $\psi(x,n)=\hat{U}^n\psi(x,0)$. The classical limit will correspond to taking $\hbar_s\to 0$ keeping $\epsilon=\tilde{\epsilon}\hbar_s/\hbar$ constant. We calculate the Husimi distribution $Q(x_0,p_0,n)$ defined by

$$Q(x_0,p_0,n)=|\langle\psi(x,n)|x_0,p_0\rangle|^2 \quad (10)$$

for a wave packet at time n. In this we take $\langle x|x_0,p_0\rangle$ as the minimum uncertainty wave packet. In the semiclassical regime, the dynamics in the Husimi representation mimics the classical dynamics of the system in phase space [9]. In Fig. 5, we show the Husimi distribution at $n=250$ from which one can clearly see that the density of Husimi distribution shows pattern similar to classical structures shown in Fig. 2.

Since $\hat{p}$ and $\hat{V}_{sq}$ in Eq. (9) do not commute, we first divide the duration between successive kicks into $N_{\triangle t}$ small time steps and the second term of Eq. (9) becomes $\Pi_{i=1}^{N_{\triangle t}}\exp\{-(i/\hbar_sN_{\triangle t})[\hat{p}^2/2+\hat{V}_{sq}]\}$. Then, we apply the split-operator method [19] to evolve the system. We use the fast Fourier transform [20] to obtain $\tilde{\psi}(p)$ from $\psi(x)$ and vice versa. In our calculations, we have taken $N_{\triangle t}\sim 2500$, the typical temporal step size is $O(10^{-3})$ and spatial step size is $O(10^{-4})$ to ensure that the evolved wave packets converged to at least eight decimal places.

The initial wave packet at $n=0$ is located in between the two barriers. We choose parameters b and $\hbar_s$ for which the Husimi distribution (shown in Fig. 5) closely resembles the classical phase space and shows that the probability density associated with the initial wave packet will ultimately leave the barrier region by predominantly following the classical path rather than by tunneling. Thus, the system stays in the semiclassical regime and tunneling is suppressed. Quite clearly, for such a choice of parameters in the semiclassical regime, the classical dynamical features would be reflected in the quantum dynamics as well.

In Secs. V and VI, we discuss some interesting dynamical features, namely, (i) the nonequilibrium steady state (NESS), (ii) classically induced suppression of diffusion, and (iii) momentum filtering which primarily arise due to coexistence of diffusive [chaotic region $(\mu<\mu_c)$] region and nondiffusive region [regular region $(\mu>\mu_c)$] in the same non-KAM system.

V. DYNAMICAL FEATURES

A. Nonequilibrium steady state

In this section, we show that the system in Eq. (1) can support NESS for intermediate time scales. We start with initial conditions uniformly distributed on a thin rectangular band around $p=0$ stretched across the well region in between the potential barriers. As the kicking field begins to impart energy to the system, the particles which absorb sufficient energy escape from the well. At any time n, the mean energy $\langle E\rangle_{in}$ of the particles lying inside the well is $\langle p_n^2/2\rangle$, where $\langle\cdot\rangle$ represents average at time n over the classical states (evolved from initial states over n kicking cycles) for which $x_l<x<x_r$. In the corresponding quantum regime, we have

$$\langle E\rangle_{in}=\int_{x_l}^{x_r}\psi^*(x,n)\frac{\hat{p}^2}{2}\psi(x,n)dx. \quad (11)$$

The effect of the operator $\hat{p}^2$ on $\psi(x,n)$ can be calculated using the fast Fourier transform and is equal to the inverse Fourier transform of $p^2\tilde{\psi}(p,n)$. Figure 6 shows that initially $\langle E\rangle_{in}$ increases and after a time scale t_r, $\langle E\rangle_{in}$ saturates to a constant. During this time scale, the behavior is similar to the classical diffusive regime of the standard map.

The existence of steady state can be understood as follows. For the parameters used in Fig. 6 the phase space in region $\mathcal{M}$ is fully chaotic. As kicks begin to act, any localized classical distribution $\rho_0(x,p)$ is quickly dispersed throughout this region. The total energy E_n of the particles in

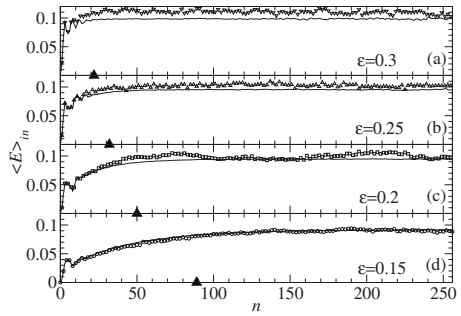

FIG. 6. Nonequilibrium steady state in the system in Hamiltonian (1). The mean energy for the particles held in between the double-barrier structure. The solid lines are the classical results and the symbols correspond to quantum results. The other parameters are $R=0.5, b=0.2, \phi=0, V_0=0.5$ and for quantum simulations $\hbar_s=0.0025$. The solid symbol (triangle up) marks the time scale t_r at which the system relaxes to the steady state.

the well region increases. Simultaneously, the particles with $|p|>p_c$ leave the finite well leading to loss of energy. Soon the loss process becomes significant and at every kick cycle the energy lost (due to barrier crossings) is more than the energy gained from the kicking potential. Thus, E_n begins to decrease. However, after the time scale t_r, the net energy change and the number of particles vary in such a manner as to maintain the mean energy $\langle E\rangle_{in}$ a constant (apart from fluctuations). This arises because the normalized momentum distribution remains nearly invariant with time as shown in Fig. 7. The chaotic mixing inside the well ensures that despite the loss of energetic particles, momentum distribution remains invariant. Thus, chaos between the barriers is essential to support the NESS. One of the factors that determine t_r is the rate at which any initial distribution of states diffuses in the chaotic region and steady-state distribution shown in Fig. 7 is achieved. This rate increases with ϵ in general. For the present case with complete chaos, one expects this rate to be proportional to $1/\epsilon^2$, just like in the diffusive regime of standard map and hence one expects $t_r \propto 1/\epsilon^2$. Numerical results shown in Fig. 6 show a good agreement with this gross estimate for t_r.

This steady state holds good until nearly all the particles have escaped out and only a fraction $q \ll 1$ remains in the well. Based on rate of diffusion in chaotic region, we can

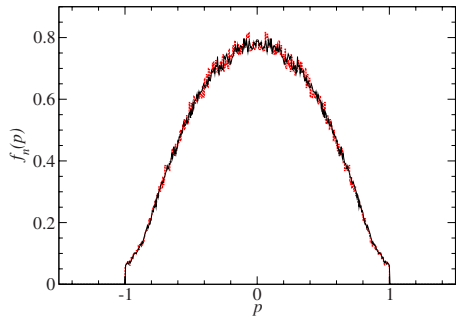

FIG. 7. (Color online) (Color Online) Classical steady-state momentum distribution for $\epsilon=0.25$ at (a) $n=100$ (solid) and (b) $n=200$ (dashed). As seen in Fig. 6(b), the steady state is reached at $n\sim 30$. The other parameters are $R=0.5, V_0=0.5, b=0.2, \phi=0$.

estimate the time at which this happens to be $t_s \propto 1/q^2\epsilon^2$. Since $q \ll 1$, we get $t_s \gg 1$. In the semiclassical regime, this mechanism carries over to the quantum dynamics as well. Notice that t_s is larger than other relevant time scales, i.e., $t_s \gg t_r > T$. Further, t_s is typically about few hundreds of kick cycles and hence we expect this to be experimentally accessible time scale as well. On a much longer time scale as $t \to \infty$, all the energetic particles escape and the steady state decays out.

Indeed, a similar nonequilibrium steady state has been experimentally observed with the periodically kicked Bose-Einstein condensate in a finite box for strong kick strengths [5]. These steady states have a classical explanation. Typically, the standard kicked rotor exhibits energy saturation and steady state for large kick strengths in the quantum regime due to destructive quantum interferences [1,2]. We emphasize that the energy saturation in our model, as well as for the BEC in finite box [5], is induced by the classical effects and leaves a trail in the semiclassical regime.

Figure 6 shows that the quantum mean energy $\langle E\rangle_{in}$ follows the classical curve quite closely. These results correspond to $\hbar_s=0.0025$ and reflect the behavior in the semiclassical regime. Larger values of ϵ correspond to moving away from semiclassical regime toward purely quantum regime. Thus, we should expect quantum averages to deviate from classical averages in a pronounced manner. This is borne out by the numerical results in Figs. 6(a)–6(c). There is current interest in quantum nonequilibrium steady states about which not much has been explored until now [21]. For $\epsilon \gg 1.0$, the quasiperiodic orbits of the standard map are sufficiently destroyed to allow global transport in phase space. Then, particles do not have to rely on discontinuities in V_{sq} to diffuse in phase space. This leads to unlimited energy absorption by the particles between the barriers and NESS is not supported. Then, the system essentially works like the kicked rotor in the strongly chaotic regime.

B. Energy saturation and steady state

As pointed out earlier, the region covered by the quasiperiodic orbits $C(\mu)$ with $\mu > \mu_c$ is nondiffusive. Now, consider curves $C_{\pm}(\mu_b)$ such that maximum value of $|p|$ for both these curves is equal to p_c as shown in Fig. 3. Then, all the curves $C(\mu)$ with $\mu < \mu_b$ will have $p \in [-p_c, p_c]$. So any state evolving on one of them will always get reflected at the barriers. Thus, to escape from the finite well, every phase-space point in the chaotic region must first reach any $C(\mu)$ with $\mu_b < \mu < \mu_c$. As time $n \to \infty$, all the particles would have escaped from the well and get locked on to one of the invariant curves $C(\mu)$ of the corresponding standard map. Thus, the momenta of escaping particles settle to a stationary distribution on $C(\mu)$ with $\mu_b < \mu < \mu_c$. Thus, the momentum distribution reaches a steady state as $n \to \infty$ and their mean energy $\langle E\rangle$ saturates to $\langle E\rangle_s$.

In Fig. 8(a), the broken curve (blue) shows $\langle E\rangle_s$ for the classical system. As this figure shows, the mean energy of the system increases with time and asymptotically approaches $\langle E\rangle_s$. In the semiclassical regime, we expect a similar behavior for the quantum average and this is shown as

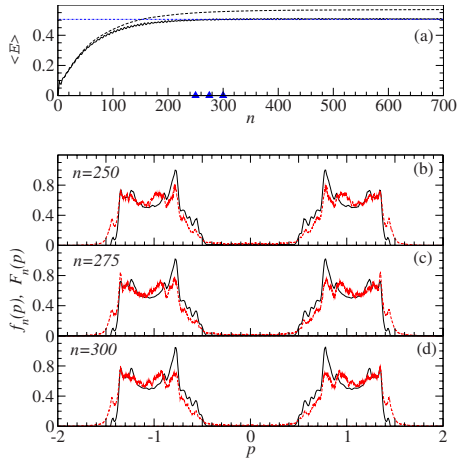

FIG. 8. (Color online) (Color Online) (a) Classical (solid line) and quantum (dashed line) mean energies as a function of time n for $\epsilon=0.3$. Other parameters are same as in Fig. 6. Numerically estimated value of $\langle E\rangle_s$ for classical system is shown as a broken line. The triangles in the x axis are the times for which momentum distribution is shown in (b)–(d). Classical (solid line) and quantum (dashed line) momentum distributions at (b) $n=250$, (c) $n=275$, and (d) $n=300$. Note that the distributions are nearly identical.

dashed curve in Fig. 8(a). The small difference in saturated values of quantum and classical mean energies can be attributed to the finiteness of Planck's constant which makes its effect felt as ε increases.

Further, Figs. 8(b)–8(d) also show the classical momentum distribution $f_n(p)$ and its quantum analog $F_n(p)=|\tilde{\psi}(p,n)|^2$ for the same set of parameters after evolving the system for $n=250$, 275, and 300 kicking periods. Probability distribution in position representation (not shown here) reveals that at $n=250$, 275, and 300 the probability density in between the barriers is negligible. Nearly identical distributions in Figs. 8(b)–8(d) mark the existence of steady state. Notice that small departures from semiclassical regime are also visible here in the form of slight difference between classical and quantum distributions. For the energy saturation effect, complete chaos between barriers is not essential. If some sticky islands are present between the barriers, the saturated classical and quantum distributions as $n\to\infty$ will display a nonzero component in the finite well region. These nonchaotic components tend to remain localized and will never escape out.

C. Momentum filtering

As demonstrated in Sec. V B, when all the chaotic particles exit from the finite well region, a steady state is reached. One possible manifestation of this asymptotic state is the momentum filtering effect that occurs for certain choices of parameters. It is possible to choose system parameters such that momentum distribution of escaped particles becomes narrow. Thus, any broad initial momentum distribution at $n=0$, after sufficient kicking periods, leads to a distinctly narrow momentum distribution. This is shown in Fig. 9. In this figure, the initial conditions are uniformly distrib-

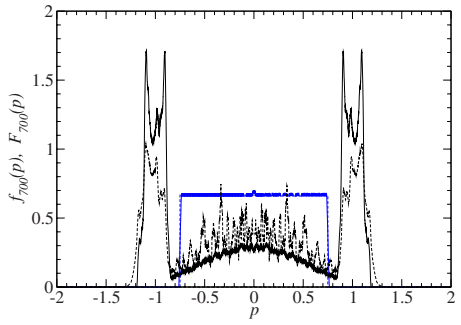

FIG. 9. (Color online) (Color Online) (a) Classical (solid line) and quantum (dashed line) momentum distributions at $n=700$ are displayed for $V_0=0.5$, $b=0.2$, $R=0.5$, and $\epsilon=0.1$. For quantum simulation, $\hbar_s=0.0025$. The initial distribution at time $n=0$ is a uniform distribution, the rectangular curve shown in blue. See text for details.

uted in the chaotic layer lying in between the barriers. This chaotic layer also ensures that the final result is independent of the details of the initial distribution. The figure shows the momentum distributions $f_{700}(p)$ (classical) and $F_{700}(p)$ (quantum) plotted for $n=700$. By this time, a large fraction of particles have escaped from the well and the distribution has become bimodal with distinct peaks near $-p_c$ and p_c. This shows that the double-barrier structure, in presence of the kicking field, acts as a momentum filter. We obtain filtering effect for a range of kick strengths (not shown here) and observe that with decrease in ϵ, the two bands in bimodal distribution become narrow. However, the time at which system approaches steady state corresponding to this bimodal distribution becomes very large. Indeed, since it is experimentally possible to design barrier heights of desired choice, it will be possible to use double-barrier structure to produce filter with desired value of p_c. In Fig. 2, we note that the escaped particles follow extremely close set of invariant curves and their speed, averaged over time, will converge to the winding number of the orbits involved. Hence, the speed distribution will have peaks of infinitesimal width at $|p_c|$. It is pertinent to note that a momentum filtering effect based on a very different mechanism has been studied by Monteiro *et al.* in the context of a variant of kicked rotor model [22].

We emphasize that all the dynamical features discussed in Secs. V A–V C can be explained on the basis of (i) coexistence of diffusive and nondiffusive regions which exists because the non-KAM nature of the system affects the dynamics differently in different phase space-regions and (ii) presence of KAM curves through out the phase space outside the double-barrier region. Hence, all the dynamical features can be attributed to the interplay between the KAM and non-KAM behaviors of the system.

VI. DISCUSSIONS AND SUMMARY

In summary, we have presented primarily numerical results of the dynamics of noninteracting particles in a double-barrier structure acted upon by periodic kicking field. This model differs from the paradigmatic kicked rotor. This is essentially a non-KAM system and hence chaotic dynamics

sets in even for infinitesimal excursions from the integrable limit of kicking strength $\epsilon=0$. Further, this displays nonequilibrium steady state and classically induced suppression of energy growth in the semiclassical regime. This is in contrast with the classical kicked rotor that displays diffusion only for $\epsilon \gg 1$ and its quantum version arrests this through dynamical localization, an outcome of quantum interferences.

Some of the earlier works on the double-barrier type potential have considered it as a scattering problem in a different setting with a drive term. For example, see Refs. [23]. An incoming wave packet hits the left barrier (see Fig. 1) and tunnels into it and, depending on the parameters chosen, some or all of it emerges out of the right barrier. This mechanism requires purely quantum effects such as tunneling and in this work we have deliberately avoided them to focus on the semiclassical regime. Since tunneling probability is nearly 0 in this semiclassical setting, any initial distribution placed anywhere outside the barriers ($|x|>a+b$) will continue to evolve on the KAM-like invariant tori. However, based on the results obtained in this paper, we can speculate about the case when quantum effects come into play. Tunneling will allow a wave packet to enter the through the left barrier and non-KAM chaos will ensure that it gets dispersed. But now, the wave packet can tunnel out through the right barrier. This scenario could potentially lead to an interesting competition between above barrier crossings and tunneling. Another interesting case relates to periodic version of this model which can also be used for directed transport. We are pursuing these questions and will be reported elsewhere.

The dynamical features in our model such as the nonequilibrium steady state and classically induced energy growth suppression are of current interest in the general context of transport and localization especially for interacting systems such as the Bose-Einstein condensates. Recently there have been several experimental results that point to classical features suppressing energy growth of condensates [14]. Typically, in such experiments, condensates are released from a confining potential and their expansion in a disordered potential is studied. When chemical potential $\mu < V_0$, where V_0 is the strength of disorder, condensates are classically reflected from the fluctuations of the disordered potential effectively localizing the condensates. In our model, particles are neither interacting nor there is any disordered potential. However, the non-KAM chaotic dynamics and KAM-like invariant curves provide the essential ingredient for the suppression of diffusion. Even as the particles are transported in the position space their energy absorption is restricted as $t \to \infty$ by KAM-like structures. Such studies form an important background to understand and clearly distinguish similar quantum phenomena such as the Anderson localization from the classically induced ones and also to explore the connections between interactions, localization, and disorder.

Quantum chaos in double-barrier potentials have been studied before experimentally using GaAs/AlGaAs heterostructures [24] though not with a periodic kicking field. In these experiments electrons tunnel through the double-barrier potential and chaos is induced within the barriers due to the field created by the charge accumulation in the well [24]. Since resonant tunneling plays an important role in this experiment, this can be regarded as being quantum in nature without classical analog. The double-barrier system in Eq. (1) could be used with resonant tunneling to study purely quantum effects as well though in the present work we have primarily explored the classical and semiclassical features. The foregoing arguments also imply that the system can also be realized experimentally in a laboratory. The cold atoms in optical lattices are the testing ground for variants of kicked rotor. For an experimental setup involving cold atoms, optical lattices with double-barrier heterostructures should be possible.

Currently there is considerable interest in the exciting field of chaotic ratchets [6]. Generally, ratchets are systems with broken spatiotemporal symmetries from which directed transport can be obtained even in the absence of a net bias. There have been several proposals and at least one experimental realization for a chaotic ratchet in the past few years. The system presented in this work lacks the spatial periodicity required of a ratchet. But the kicking potential, being sinusoidal, is already spatially periodic. Further, from a theoretical perspective, it is not difficult to have spatially periodic double-barrier structures. Then, it might become possible to realize ratchet dynamics in this system. All the existing chaotic ratchet proposals are based on systems that obey KAM theorem. The model presented in this work might lead to new ways to use non-KAM type dynamics for deterministic directed transport.

ACKNOWLEDGMENTS

The authors acknowledge many useful discussions with Dilip Angom during the course of this work. Numerical calculations for quantum system are carried out on PRL 3TFLOP cluster computer. One of the authors (H.P.) thanks Manjunatha of CDAC and computer center staff for suggestions and assistance in efficiently using cluster computer.

APPENDIX A

Considering a particle that evolves on an invariant curve of the standard map $C_5(\mu_5)$ approaches right barrier at $x_w = R\pi$, with $p > p_c$ during its motion after nth kick, crosses it, and exits onto another invariant curve of standard map $C_6(\mu_6)$. In this appendix, we show that as the width of the barrier $b \to 0$, $C_5(\mu_5) \to C_6(\mu_6)$.

After the particle crosses the interface at x_w and if Δt denotes the time it will take to cross the barrier region of width b, then $\Delta t \to 0$ if $b \to 0$. Hence, the probability that a particle will experience the next kick while crossing the barrier will also tend to zero. Hence, we can assume that the particle does not experience a kick while crossing the barrier. In such a situation, the particle will face only two discontinuities between nth and $(n+1)$th kicks. Thus, $k=2$, $B_1 = x_w$, and $B_2 = x_w + b$. From our assumptions, $\binom{x_n^0}{p_n^0}$ lie on $C_5(\mu_5)$ and $\binom{x_n^2}{p_n^2}$ will lie on $C_6(\mu_6)$.

$$\begin{pmatrix} x_n^1 \\ p_n^1 \end{pmatrix} = \hat{\mathcal{R}}_1 \begin{pmatrix} x_n^0 \\ p_n^0 \end{pmatrix} \Rightarrow \begin{pmatrix} x_w + \dfrac{(x_n^0 - x_w)p_n^1}{p_n^0} \\ \sqrt{(p_n^0)^2 - 2V_0} \end{pmatrix}. \quad \text{(A1)}$$

Similarly,

$$\begin{pmatrix} x_n^2 \\ p_n^2 \end{pmatrix} = \hat{\mathcal{R}}_2 \begin{pmatrix} x_n^1 \\ p_n^1 \end{pmatrix} \Rightarrow \begin{pmatrix} x_w + b + \dfrac{(x_n^1 - x_w - b)p_n^2}{p_n^1} \\ \sqrt{p_n^{1^2} - 2V_0} \end{pmatrix}. \quad \text{(A2)}$$

Substituting for x_1 and p_1 from Eq. (A1) in Eq. (A2), we get

$$\begin{pmatrix} x_n^2 \\ p_n^2 \end{pmatrix} = \begin{pmatrix} b - \dfrac{bp_n^0}{p_n^1} + x_n^0 \\ p_n^0 \end{pmatrix}. \quad \text{(A3)}$$

Using $b \to 0$, we get $\binom{x_n^2}{p_n^2} \to \binom{x_n^0}{p_n^0}$. This implies $C_5(\mu_5) \to C_6(\mu_6)$ or $\mu_6 - \mu_5 \to 0$.

APPENDIX B

We show that for certain special choices of (R, ϕ), reflection from the walls of potential V_{sq} takes a state from invariant curve C_+ to its symmetric counterpart C_-, where C_+ and C_- are related through reflection symmetry about (0,0). Let

$$\left\{ \begin{matrix} R\pi + \phi = l\pi \\ -R\pi + \phi = m\pi \end{matrix} \right\}, \quad l,m \in \text{integer}. \quad \text{(B1)}$$

Then, $x_r = l\pi$ and $x_l = m\pi$. Let $\binom{x_n^{i-1}}{p_n^{i-1}}$ lie on C_+. Reflection from the right boundary at x_r will take it to

$$\begin{pmatrix} x_n^i \\ p_n^i \end{pmatrix} = \hat{\mathcal{R}}_i \begin{pmatrix} x_n^{i-1} \\ p_n^{i-1} \end{pmatrix} = \begin{pmatrix} 2l\pi - x_n^{i-1} \\ -p_n^{i-1} \end{pmatrix} \quad \text{(B2)}$$

on the invariant curve C. The spatial periodicity of 2π in the standard map implies that

$$\begin{pmatrix} (2l\pi - x_n^{i-1}) \bmod (2\pi) \\ -p_n^{i-1} \end{pmatrix} = \begin{pmatrix} -x_n^{i-1} \\ -p_n^{i-1} \end{pmatrix} \quad \text{(B3)}$$

is on C. Since $\binom{-x_n^{i-1}}{-p_n^{i-1}}$ is on C_- and C_- is unique, we have $C = C_-$. Thus, the effect of reflection from the right boundary at x_r is to take a state from C_+ to C_- if Eq. (B1) is satisfied. Similarly, the effect of reflection from left boundary at $-x_l$ is to take a state from C_- to C_+.

[1] B. V. Chirikov, Phys. Rep. **52**, 263 (1979); F. M. Izrailev, *ibid.* **196**, 299 (1990); G. Casati, *Quantum Chaos: Between Order and Disorder* (Cambridge University Press, Cambridge, 1995).

[2] B. V. Chirikov, in *Chaos and Quantum Physics*, edited by M.-J. Giannoni, A. Voros, and J. Zinn-Justin (North-Holland, Amsterdam, 1991).

[3] L. E. Reichl, *The Transition to Chaos: Conservative Classical Systems and Quantum Manifestations* (Springer, New York, 2004).

[4] G. Casati, B. V. Chirikov, F. M. Izraelev, and J. Ford, Lect. Notes Phys. **93**, 334 (1979); S. Fishman, D. R. Grempel, and R. E. Prange, Phys. Rev. Lett. **49**, 509 (1982).

[5] F. L. Moore, J. C. Robinson, C. Bharucha, P. E. Williams, and M. G. Raizen, Phys. Rev. Lett. **73**, 2974 (1994); F. L. Moore, J. C. Robinson, C. F. Bharucha, B. Sundaram, and M. G. Raizen *ibid.* **75**, 4598 (1995).

[6] T. Salger *et al.*, Science **326**, 1241 (2009); A. Kenfack, J. Gong, and A. K. Pattanayak, Phys. Rev. Lett. **100**, 044104 (2008); S. Flach, O. Yevtushenko, and Y. Zolotaryuk, *ibid.* **84**, 2358 (2000); H. Schanz, M. F. Otto, R. Ketzmerick, and T. Dittrich, *ibid.* **87**, 070601 (2001); T. S. Monteiro, P. A. Dando, N. A. C. Hutchings, and M. R. Isherwood, *ibid.* **89**, 194102 (2002); E. Lundh and M. Wallin, *ibid.* **94**, 110603 (2005); J. Gong and P. Brumer, *ibid.* **97**, 240602 (2006).

[7] G. M. Zaslavsky, *Hamiltonian Chaos and Fractional Dynamics* (Oxford University Press, Oxford, 2005).

[8] R. Sankaranarayanan, A. Lakshminarayan, and V. B. Sheorey, Phys. Rev. E **64**, 046210 (2001); Phys. Lett. A **279**, 313 (2001).

[9] K. Takahashi and N. Saiton, Phys. Rev. Lett. **55**, 645 (1985).

[10] B. Hu, B. Li, J. Liu, and Y. Gu, Phys. Rev. Lett. **82**, 4224 (1999).

[11] T. M. Fromhold *et al.*, Nature (London) **428**, 726 (2004); T. M. Fromhold, A. A. Krokhin, C. R. Tench, S. Bujkiewicz, P. B. Wilkinson, F. W. Sheard, and L. Eaves, Phys. Rev. Lett. **87**, 046803 (2001).

[12] S. A. Gardiner, J. I. Cirac, and P. Zoller, Phys. Rev. Lett. **79**, 4790 (1997).

[13] K. Henderson *et al.*, Europhys. Lett. **75**, 392 (2006).

[14] D. Clément, A. F. Varón, M. Hugbart, J. A. Retter, P. Bouyer, L. Sanchez-Palencia, D. M. Gangardt, G. V. Shlyapnikov, and A. Aspect, Phys. Rev. Lett. **95**, 170409 (2005); C. Fort, L. Fallani, V. Guarrera, J. E. Lye, M. Modugno, D. S. Wiersma, and M. Inguscio, *ibid.* **95**, 170410 (2005); T. Schulte, S. Drenkelforth, J. Kruse, W. Ertmer, J. Arlt, K. Sacha, J. Zakrzewski, and M. Lewenstein, *ibid.* **95**, 170411 (2005); L. Sanchez-Palencia *et al.*, New J. Phys. **10**, 045019 (2008).

[15] T. P. Meyrath, F. Schreck, J. L. Hanssen, C. S. Chuu, and M. G. Raizen, Phys. Rev. A **71**, 041604(R) (2005).

[16] D. Poletti, L. Fu, J. Liu, and B. Li, Phys. Rev. E **73**, 056203 (2006).

[17] B. Galdrikian, B. Birnir, and M. Sherwin, Phys. Lett. A **203**, 319 (1995).

[18] Paul Harrison, *Quantum Wells, Wires and Dots* (Wiley, West Sussex, 2005).

[19] D. J. Tannor, *Introduction to Quantum Mechanics: A Time Dependent Perspective* (University Science Books, Sausalito, 2007).

[20] Fastest Fourier transform in the west: www.fftw.org

[21] M. Žnidarič, J. Stat. Mech.: Theory Exp. (2010) L05002.

[22] T. Jonckheere, M. R. Isherwood, and T. S. Monteiro, Phys. Rev. Lett. **91**, 253003 (2003).

[23] M. Gärttner, F. Lenz, C. Petri, F. K. Diakonos, and P. Schmelcher, Phys. Rev. E **81**, 051136 (2010); M. Wagner, Phys. Rev. A **51**, 798 (1995); I. Vorobeichik, R. Lefebvre, and N. Moiseyev, Europhys. Lett. **41**, 111 (1998); M. Wagner, Phys. Rev. B **49**, 16544 (1994); For two barrier quantum pumps, see M. M. Mahmoodian, L. S. Braginsky, and M. V. Entin, *ibid.* **74**, 125317 (2006).

[24] G. Jona-Lasinio, C. Presilla, and F. Capasso, Phys. Rev. Lett. **68**, 2269 (1992); C. Presilla, G. Jona-Lasinio and F. Capasso, Phys. Rev. B **43**, 5200(R) (1991); A. J. McNary and A. Puri, J. Appl. Phys. **80**, 247 (1996); A. Rosa, A. Puri, J. E. Murphy, and T. Odagaki, *ibid.* **75**, 5196 (1994).